A Perspective on the Reliability of MEMS-Based Components for Telecommunications

John C. McNulty*
DfR Solutions LLC, 5110 Roanoke Place, College Park, MD, USA

ABSTRACT

Despite the initial skepticism of OEM companies regarding reliability, MEMS-based devices are increasingly common in optical networking. This presentation will discuss the use and reliability of MEMS in a variety of network applications, from tunable lasers and filters to variable optical attenuators and dynamic channel equalizers. The failure mechanisms of these devices will be addressed in terms of reliability physics, packaging methodologies, and process controls. Typical OEM requirements will also be presented, including testing beyond of the scope of Telcordia qualification standards. The key conclusion is that, with sufficiently robust design and manufacturing controls, MEMS-based devices can meet or exceed the demanding reliability requirements for telecommunications components.

Keywords: MEMS, tunable laser, tunable filter, VOA, DCE, reliability, optical, Telcordia

1.0 INTRODUCTION

MEMS-based devices have been used for decades in applications like accelerometers and other sensors, demonstrating high reliability in demanding environments. More recently, Texas Instrument's digital micro-mirror devices (DMD) have enabled the successful deployment of over 1.5 million light projection systems, with estimated mean lifetimes of over 50 years [1]. In the telecommunications industry, the use of MEMS-based devices has proliferated over the past ten years, with applications in optical switching [3,7], tunable lasers and filters [2-5], optical cross-connects, attenuators, add/drop multiplexers, and DWDM [6].

There is a growing body of literature on the fundamental materials properties and size effects of MEMS structures [8-11], as well as their performance in extended cycling [12-13] and extreme shock and vibration environments [14-16]. However, given the wide variety of MEMS device structures and their relevant failure modes, there is a general lack of MEMS-specific qualification test requirements. In the absence of standardized testing, more extensive knowledge of failure modes, and the associated reliability of MEMS-based devices, many OEMs have developed their own requirements for device manufacturers.

2.0 MEMS STRUCTURES AND PROCESSING

The author has worked with two main types of MEMS structures: comb-driven actuators and diffractive mirrors. Both structures are composed of single crystal silicon and produced using deep reactive ion etching (DRIE), with typical out-of-plane thicknesses less than 100 microns and minimum in-plane thicknesses of comb and support elements of 5 microns. Scanning electron micrographs of each structure are shown in **Figures 1** and **2**.

* jmcnulty@dfrsolutions.com; 415-806-7704

Reliability, Packaging, Testing, and Characterization of MEMS/MOEMS VII, edited by Allyson L. Hartzell, Rajeshuni Ramesham, Proc. of SPIE Vol. 6884, 68840B, (2008) · 0277-786X/08/$18 · doi: 10.1117/12.773640

The actuator structures are used to move adhesively-attached mirrors that are also produced by DRIE etching. The first structure (**Fig. 1(a)**) is used in a Fabry-Perot tunable laser with a Littman-Metcalf external cavity, where the cavity is defined by the distance between the laser diode facet, grating, and MEMS mirror. The second structure (**Fig. 1(b)**) is used to modify the optical path length in a tunable filter. Both devices have closed loop control (the first with feedback from a wavelength locker subassembly, and the second with position detection off of the back surface of the mirror with a LED/split detector subassembly), and each enables tuning over 100+ channels of the C and/or L band, with 25 to 50 GHz channel spacing. The MEMS structures of both devices are co-packaged with other optical subcomponents and then hermetically sealed in conventional butterfly packages.

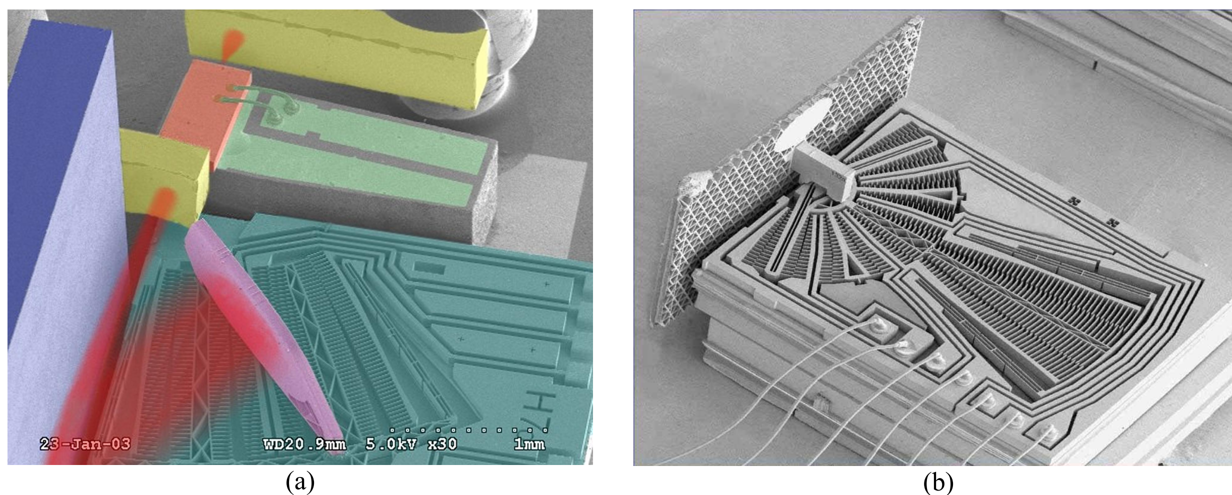

(a) (b)

Figure 1: MEMS actuators for (a) tunable lasers and (b) tunable filters/receivers.

The diffractive mirror structures are used in variable optical attenuators (VOAs, **Fig. 2(a)**) and dynamic channel equalizers (DCEs, **Fig. 2(b)**). In both cases, the optical beam path is perpendicular to the plane of the MEMS structures, and the mirrors tilt out of plane to affect attenuation of the reflected optical power. The VOA attenuates wavelengths more or less equally, whereas the DCE selectively attenuates up to 100 independent wavelengths spaced over the C and/or L band, similar to the tunable laser and filter. The MEMS components of each device are packaged individually into hermetic subassemblies (TO cans and 96-pin packages, respectively), and then integrated into larger structures.

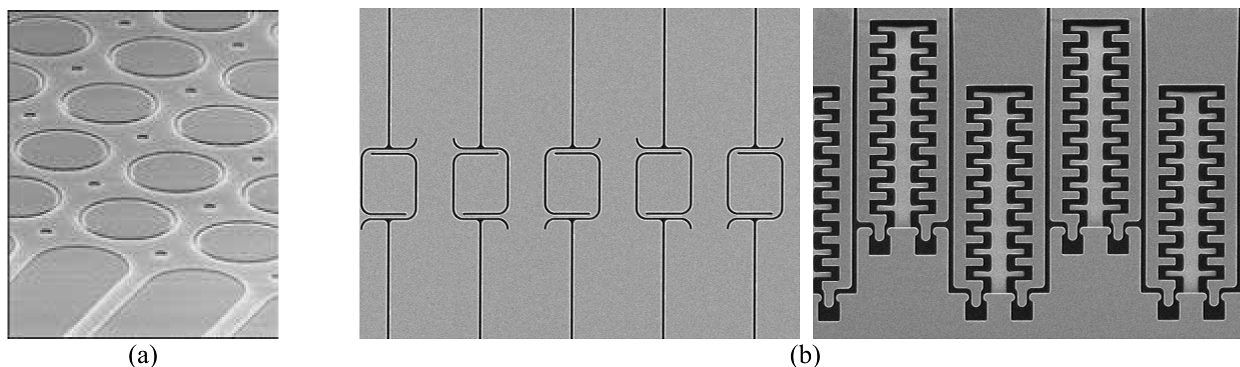

(a) (b)

Figure 2: Diffractive MEMS structures for (a) VOAs and (b) DCEs (showing both the mirror pivots and combs).

3.0 MEMS FAILURE MECHANISMS

There are a variety of failure mechanisms that can affect the reliability of MEMS structures: flaw sensitivity (arising from low fracture toughness) and the associated size dependence of strength, fatigue, stiction, wear, and stress corrosion cracking (due to water vapor). Depending on the MEMS design, stiction and wear may be eliminated – all of the structures discussed in **Section 2** are non-contacting except in extreme shock and vibration events. Since elevated water vapor concentrations tend to exacerbate all failure mechanisms (stiction is usually inhibited by adsorbed water), the vast majority of MEMS devices in telecom applications are hermetically packaged. Fatigue can be effectively eliminated by maintaining a sufficient margin of safety between the design stresses and the stress associated with the fatigue crack growth threshold.

The fracture toughness of DRIE structures is roughly equivalent to that of bulk single crystal silicon. Literature values are below 1.0 MPa√m independent of the cleavage plane [11], compared to values as high as ~4 MPa√m for polycrystalline silicon. The higher values for polysilicon are due to grain boundary toughening and other crack deflection mechanisms; such mechanisms are completely absent in single crystal silicon. The generic relationship between fracture toughness, K_c, strength, σ_c, and flaw size, a, is given by:

$$K_c = Y \cdot \sigma_c \cdot \sqrt{\pi a} \qquad (1)$$

where Y is a geometric factor that varies with loading conditions and sample size. Since fracture toughness is generally constant (in the absence of environmental factors), the strength is controlled by surface defects (either etching defects or intentional stress concentrators), as compared to both surface and bulk defects for polycrystalline silicon.

Size dependence of strength is a direct consequence of flaw sensitivity, since the likelihood on encountering a critical flaw increases as the surface area (or volume, for materials with bulk defects) increases. The failure probability, P_s, as a function of stress, σ, and surface area, A, is generally described using a two-parameter Weibull distribution of the form:

$$P_s(A) = \exp(-(A/A_o) \cdot (\sigma/\sigma_o))^m \qquad (2)$$

where m and σ_o are the Weibull shape parameter and reference strength, respectively, and A_o is the sample surface area on which both are experimentally determined. Both the strength and Weibull modulus vary significantly based on the surface roughness and defect density, but generally values of 1.2 to 8 GPa and 2.7 to 12, respectively, can be obtained with secondary processes to improve sidewall quality [9,10].

The impact of MEMS element size and geometry on the resulting strength of simple unnotched and notched cantilever structures is shown in **Figure 3**, using data adapted from Minoshima *et al* [9]. The increasing spread in strength values as cantilever dimensions decrease is likely an impact of both slight variations in the nominal dimensions due to etching variations as well as the diminishing difference between surface flaw size and sample dimensions (a ratio of ~0.002 for the largest cantilever and ~0.1 for the smallest). The notches used in that study simulate single surface defects, and provide a vivid illustration of the effect of surface quality on strength – see **Figure 5** for images of typical sidewall quality.

Water vapor- and particulate-induced shorting (or blocking) of comb and diffractive MEMS structures are not intrinsic mechanisms, but nonetheless are likely the most commonly observed types of failures. Water vapor-induced failures can be eliminated using conventional hermetic packaging techniques, and hence such failures are strong indicators of poor process control and/or package design. Reduction of particulates in packaged devices is more difficult for a number of reasons: first, the silicon MEMS device itself is a large source of particulates, either as slivers from roughly-etched

sidewalls that break loose during contact or as chips broken off from device edges and surfaces during handling; second, particulates from other ceramic, metallic, or glass subcomponents (arising from handling) are common even in well-controlled cleanroom environments. As discussed in **Sections 4** and **5**, more extensive screening tests are required to reduce the impact of particulates.

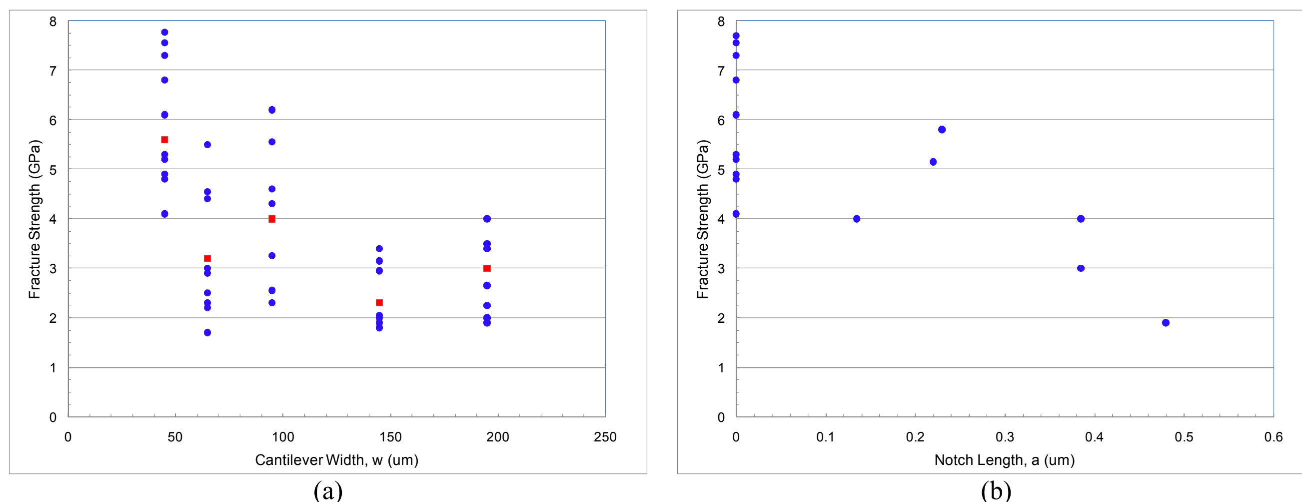

(a) (b)

Figure 3: Measured fracture strength of etched single crystal Si as a function of (a) cantilever width and (b) notch depth (adapted from Minoshima *et al.* [9]).

4.0 MEMS DESIGN, SCREENING, AND QUALIFICATION ISSUES

Much like any active opto-electronic component, substantial design, process control, and qualification testing is required to produce a reliable MEMS-based component. One of the goals of this paper is to highlight key test techniques during the development process, and thereby provide guidance for future MEMS-based telecom devices. Descriptions of various analyses, measurements, and tests are detailed in **Table 1** below.

Mechanical design and finite element analysis (FEA) software packages are indispensable tools for MEMS development. The most recent packages explicitly address surface roughness effects to identify the locations of highest stress concentration and subsequent fracture, which, as discussed in **Section 3**, are critical to evaluating MEMS processing parameters and their impact on flaw size distributions & subsequent fracture locations. On-wafer test structures and SEM or interferometric measurements of surface quality can then be used to provide accurate process capability assessments of material quality both within a given wafer and across multiple wafer lots. Relatively simple FEA analyses of a typical on-wafer test structure are shown in **Figure 4**. Representative SEM micrographs of wafers produced with two different processes are presented in **Figure 5**, overlayed on a graph showing the cumulative failure distributions (fracture load, as applied to the center of the structure in **Figure 4(a)**) for multiple test structures on each wafer. In this example, the fracture load in grams is roughly equivalent to the fracture stress in GPa. The values are consistent with those reported in other studies [9, 10].

Table 1: Summary of analysis and testing performed during development of MEMS devices for telecom applications.

Development Step	Description and Objectives
Design	• Mechanical/finite element analysis: dimensional parametric studies to assess resonant frequencies, peak stresses, and critical feature/flaw sizes
Process Development & Control	• Wafer processing: SEM/interferometry of etch quality on actual and test structures; adhesion and strength measurements on test structures • Actuation characterization: curve tracer measurements of displacement as a function of I/V
Evaluation	• Swept-frequency vibration (operational and non-operational): confirm resonant frequencies; assess optical performance variation; iterative development of closed loop controls (if necessary) • MEMS on submount: stepped shock testing to failure (500-5000 g+ acceleration) to identify functional limits
Screening	• MEMS on submount: "proof" testing at 750 g+ acceleration to identify low level defects • Device: "proof" testing at 500 g+ acceleration to identify low level defects • Random locking (fixed or variable frequency): assess stability of actuator movement, particularly particulate-induced blockage or shorting
Qualification (per relevant Telcordia standard)	• Operational vibration (5 g, 10-100 Hz; 2 g, 100-500 Hz): GR-468 • Non-operational vibration (20 g, 20-2000 Hz): GR-468,-1073, and -1221 • Operational shock (10g, 0.3 msec half sine; customer requirements up to 50 g, 0.1 msec half sine): GR-468 • Non-operational shock (500 g, 1 msec half sine with TEC; 1500 g, 1 msec half sine with no TEC): GR-468;-1073, and -1221 • Endurance locking/actuation (10 k-10 M cycles): GR-1073

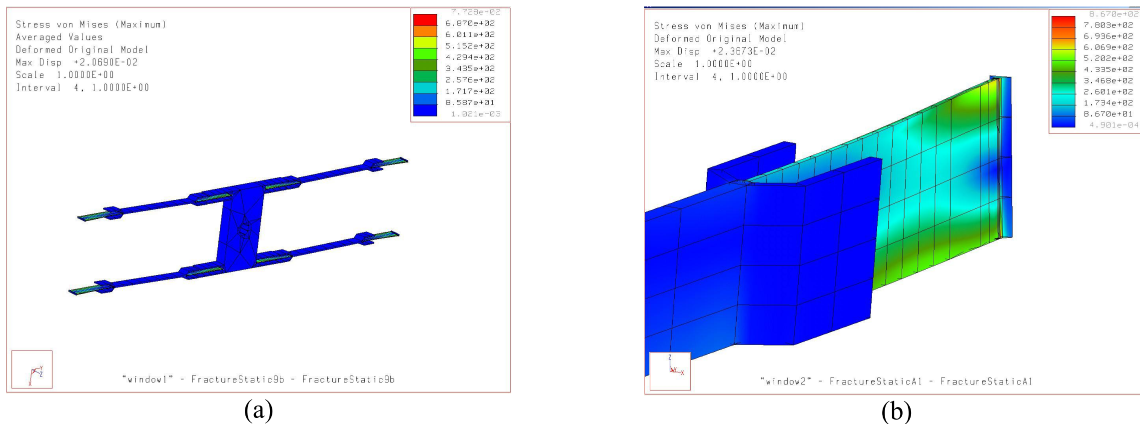

Figure 4: Typical FEA analysis of an actuator test structure, indicating the location of maximum stress. Note that these calculations do not explicitly account for surface roughness and defects, but that such can easily be implemented in FEA as a design/verification tool.

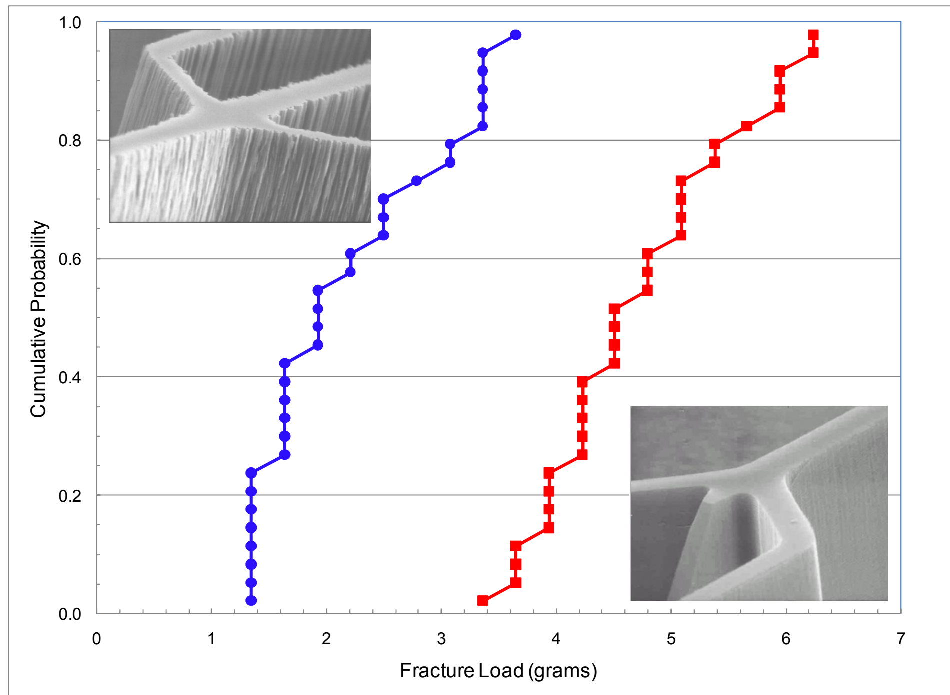

Figure 5: Fracture loads of on-wafer test structures as a function of sidewall quality. The test structure geometry is shown in **Figure 4**.

An example of swept frequency vibration testing on the tunable laser device is shown in **Figure 6**. In this particular example, the acceleration profile follows that of typical qualification testing, where laser stability is measured through variations in the output wavelength (arising from MEMS vibration and cavity length changes); in other designs, output power may be a more sensitive metric [5]. In open loop operation (top graph), significant resonances are observed near 200 Hz (within typical specified vibration ranges for Telcordia) and slightly below 3 kHz (which can be induced during operational shock). The bottom graph demonstrates how closed loop control can dampen these resonances and significantly stabilize tunable laser output.

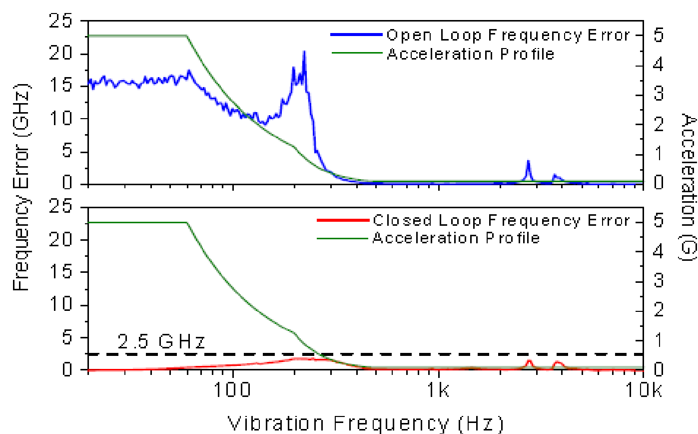

Figure 6: MEMS performance of tunable laser during vibration under open-loop and closed-loop control.

Given that wafer test structures and SEM measurements provide only a limited snapshot of overall wafer quality and that subsequent MEMS damage can occur due to handling, evaluation and screening tests need to be performed at the MEMS and package-level to ensure reliable performance. Stepped-acceleration shock tests on multiple devices from a given wafer help to identify damage thresholds for the actual device structure. Proof testing at levels above expected field conditions (500 to 1,500 g, depending on whether or not thermo-electric coolers (TECs) are used in the device) provides further assurance that there are no 'quality escapes' due to low-level defect concentrations on the wafer. The sampling levels of both types of tests can be reduced if no failures are observed and/or significant correlation is established with the test structure results and SEM observations. The (not insignificant) limitations of shock testing are relative uncertainty of actual acceleration values at the MEMS level as well as the difficulty of testing enough samples per test run to not sacrifice production throughput.

To date, there are no explicit Telcordia requirements for MEMS-based devices. However, due to increasingly prevalent special testing required by OEMs, implicit requirements were added into the latest revision of GR-468-CORE (Issue 2) to address operational shock and vibration. The conditions were based on shock events observed on operational line cards during adjacent line card insertions (to account for worst-case conditions during installation) as well as vibrations associated with usage and earth movements (adjusted to account for amplification of accelerations due to rack compliance). An example of actual measurements taken during line card insertion is shown in **Figure 7(a)**, with the associated customer-specified operational shock condition requirements shown in **Figure 7(b)**. The Telcordia conditions for operational shock represent the lowest common denominator of special OEM requirements (10 g acceleration with a 0.3 msec pulse), whereas the most aggressive OEM-specified conditions range up to 50 g acceleration with a 0.1 msec pulse. The OEM-specified conditions for operational vibration are also typically higher than the Telcordia requirement due to substantial variations from manufacturer to manufacturer in rack compliance.

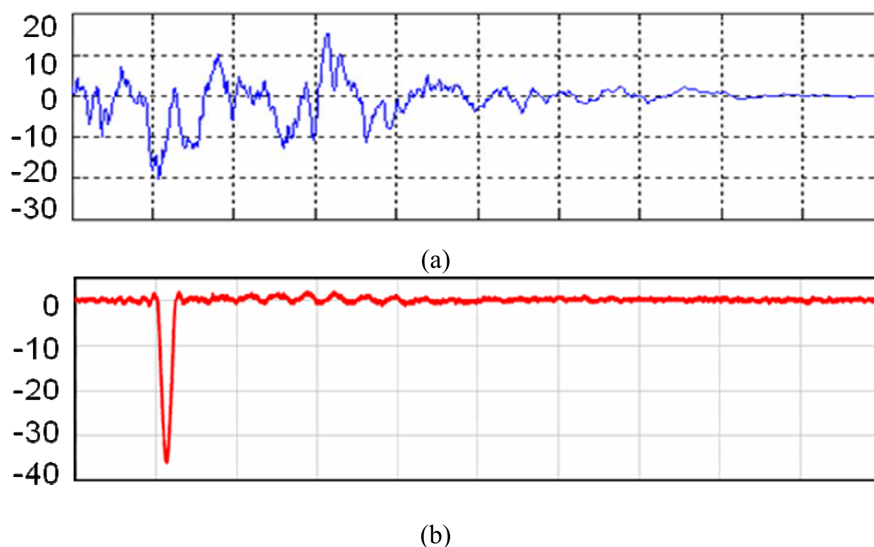

Figure 7: Measured acceleration spectra during (a) line card insertion and (b) customer-specified 35g operational shock test. The vertical axis is acceleration in g's, and the horizontal axis is time (1 msec/division).

Some OEMs specify 'endurance switching' testing for MEMS devices, similar to the requirements of GR-1073-CORE for optical switches. Section 5 of that document indicates required durations of 10,000 cycles, with conditional requirements up to 1,000,000 cycles. However, OEMs may specify variations on that test for multi-channel devices, involving sequential switching (up and down the channel range) and/or random switching with possible variable frequency. For MEMS-based devices involving physical contact of the MEMS surfaces, such testing should be regarded

as a requirement for device suppliers due to concerns regarding stiction and/or generation of wear debris (with subsequent erosion and fracture of the structure). For non-contacting MEMS devices, the requirements should be based on an analysis of the peak stresses experienced during operation and anticipated shock/vibration events as well as the relative humidity in the device package to address the risk of fatigue. For hermetically sealed devices, the fatigue threshold for single crystal silicon is generally greater than 90% of the pristine fracture strength, and studies have demonstrated the lack of stress corrosion cracking-assisted fatigue in such environments [13]. Hence, fatigue fracture can be explicitly addressed through design of the MEMS device, and suppliers may thereby use theoretical arguments in lieu of actual testing. However, some level of endurance testing is still recommended to satisfy OEM concerns.

5.0 QUALIFICATION AND LONG-TERM RELIABILITY RESULTS

Many authors have reported generic reliability data for MEMS-based telecom devices, in the form of either pass/fail numbers in individual tests (invariably only reporting results when all units passed) or extrapolated reliability estimates using limited test data. One important aspect of this paper is the opportunity to report Telcordia & special test data as well as actual field data on deployed devices. While the following results pertain only to the tunable laser using the MEMS structure shown in **Figure 1(a)**, some general comments will be made regarding the other devices mentioned in **Section 3**.

A summary of Telcordia, field deployment, and special test results is presented in **Tables 2** and **3**. For the first generation design of the tunable laser device, failures occurred during a variety of the tests required by GR-468-CORE. However, none of these failures occurred due to MEMS, but rather commonly encountered device packaging issues.

Field deployment of a larger population of lasers revealed additional failure modes, only two of which related to MEMS. The first was due to water vapor condensation on, and subsequent shorting of, the MEMs actuator. During failure analysis, the internal water vapor level was measured at >80,000 ppm, which is sufficient to cause condensation on the actively cooled MEMS structure at case temperatures above ambient; upon cooling, the operation of both failed MEMS devices recovered due to evaporation of the condensed water . The true root cause of failure was solder joint fracture around the package window, allowing ingress of water vapor above of the nominal level of ~3,000 ppm. The second observed failure mode was particulate-induced shorting of the actuator. The source of the particulate was not definitively identified, but could have been handling-induced chipping of the MEMS and other subcomponents, or from outside of the package prior to sealing.

Substantial process improvements were made to the second generation design, with additional inspection steps to reduce initial particulate concentrations. Furthermore, shock and vibration screening tests were added to identify weak structures as well as stimulate particulate movement within the package, thereby inducing potential failures before final module testing. As a result of all of these improvements, the tunable laser passed all Telcordia GR-468 tests during initial qualification and subsequent requalification.

Field deployment of a much larger population of second generation lasers revealed some old and new failure modes. Additional devices failed due to particulate-induced shorting (though at roughly half the failure rate of the first generation), and one device failed due to fracture of a suspension in the MEMS structure. The fractured actuator may have had initial defects that were not effectively identified (or perhaps even induced) by shock and vibration screening. Given the uncertainty of actual field shock conditions, previous evidence of rough handling of other lasers, and the demonstrated endurance performance of the MEMS structure (**Table 3**), handling-induced damage in the field was nonetheless believed to be the root cause. Most notably, *the greatest number of field failures was attributed to subcomponents on the tunable laser driver board*, including capacitors, FETs, and ICs.

Table 2: Summary of Telcordia and field deployment failures in two generations of a tunable laser product, with the associated root causes.

Device Design	Condition	Units Tested	Failures (in test)	MEMS Failures	Root Cause
Generation 1	Telcordia GR-468	129	4 (accelerate aging)	0	Diode drift
			1 (high temp storage)	0	Alignment shift (adhesive)
			1 (damp heat storage)	0	Alignment shift (adhesive)
			1 (thermal cycling)	0	Adhesive debonding
			3 (mechanical shock)	0	Adhesive debonding
			2 (non-op vibration)	0	Wirebond failure
	Field Deployment	368	5	0	Pigtail weld fracture
			5	0	Alignment shift (adhesive)
			5	0	Adhesive debonding
			3	2	Package leak (shorting)
			1	0	Wirebond failure
			1	1	Particulate shorting
Generation 2	Telcordia GR-468	251	0	0	
	Field Deployment	5,300+	14	0	PCBA component failure
			7	7	Particulate shorting
			1	1	Suspension fracture

Table 3: Constant frequency fatigue qualification testing on MEMS actuators in a tunable laser product. N and N_f are the total sample size and number of failures, respectively. The reliability estimate (FIT) is in failures per billion cycles, rather than hours.

Test	N	N_f	Cumulative Cycles	FIT @ 90% Confidence
Endurance cycling at 200 Hz and 25ºC (ambient humidity, ~50%)	20	0	95,000,000,000	< 1

The subcomponent failure rates are summarized in **Table 4**, based on estimated field deployment hours. It is difficult to strictly categorize each as "infant mortality" (decreasing rate with time) or "random" (constant failure rate): the particulate-induced failures would traditionally be labeled the former, since particulates are invariably pre-existing defects, whereas the PCBA component and MEMS fracture failures could be induced by a combination of pre-existing defects (for example, voids in capacitors or larger etch defects in MEMS) and aggressive field conditions ("acts of god & war" that typically define random failure). Nonetheless, the modes are treated as equal for comparison. Some key conclusions are:

- The failure rates for the PCBA components are likely overestimates due to relatively limited field hours, but generally consistent with test data from the component manufacturers and/or generic estimates from Telcordia SR-332.
- Particulate-induced failure is the most prevalent MEMS-based failure mode, but the failure rate is still comparable to that of the much more heavily deployed PCBA components.
- The failure rate due to comb fracture is likely an anomaly due to unknown field conditions, but again comparable with the PCBA components.
- The overall failure rate of the MEMS-based tunable laser module (~600 FITs at 90% confidence) is similar to that of many more mature opto-electronic components, while possessing much greater complexity and utility.

Table 4: Summary of MEMS and PCBA component failure rates in a Telcordia-qualified tunable laser product. FIT is defined as failures per billion hours.

Devices Shipped	5,300+		
Cumulative Field Hours	49,000,000+		
Failure Type	Description	Occurrence	FIT @ 90% confidence, 25ºC
Packaging-Induced	MEMS: shorting or blockage due to particulates	7	240
Subcomponent	PCBA components (capacitors, diodes, FETs, potentiometers, oscillators, and ICs)	14	79-215 (per component); 410 (total)
	MEMS: comb fracture	1	79

The field reliability of MEMS devices in the other products (tunable filters, VOAs, and DCEs) is generally comparable to that of the tunable laser. Design and packaging similarity of the tunable filter (hundreds shipped) with the tunable laser leads to the same failure modes and overall occurrence rates. The MEMS-based VOAs are much more heavily deployed (>100,000 units shipped), and the only observed failure mode for the diffractive MEMS structure is water vapor-induced shorting due to package leaks in the TO can and subsequent water vapor ingress. Improvements to the sealing process have substantially reduced the occurrence of such failures. Failures in the DCE (hundreds to thousands shipped) from MEMS fractures have been directly attributable to excessive handling damage during transport, installation, and/or use.

6.0 CONCLUSIONS

The use of MEMS-based components is proliferating in the telecommunications industry. MEMS structures exhibit a variety of failure mechanisms, but many can be eliminated through design and existing packaging methods. The occurrence of the remaining mechanisms can be reduced or eliminated with sufficient evaluation and screening tests. Specific and anecdotal results for a number of MEMS-based opto-electronic components demonstrate that such devices can meet or exceed the demanding reliability requirements of telecom OEMs.

Acknowledgments

The author would like give special thanks to Hal Jerman and Joe Drake of Coherent, Inc., for valuable discussions, data, and analysis, as well as Kevin Yasamura of FormFactor and Jocelyn Nee of NeoPhotonics for discussion of MEMS designs and testing.

References

1. M.R. Douglas, “DMD Reliability: a MEMS Success Story,” *Proceedings of the SPIE*, 4980 (2003).
2. H. Jerman and J.D. Grade, “A Mechanically-Balanced DRIE Rotary Actuator for a High-Power Tunable Laser,” Technical Digest 2002 Solid State Sensor and Actuator Workshop, Hilton Head, SC, 7-10 (2003).
3. J.D. Grade, H. Jerman, and T.W. Kenny, “A large-deflection electrostatic actuator for optical switching applications,” Technical Digest 2000 Solid State Sensor and Actuator Workshop, Hilton Head, SC, 97-100 (2000).
4. J.D. Berger and D. Anthon, “Tunable MEMS Devices for Optical Networks,” *Optics and Photonics News*, March, 43-49 (2003).

5. B. Pezeshki, E. Vail, J. Kubicky, G. Yoffe, S. Zou, J. Heanue, P. Epp, S. Rishton, D. Ton, B. Faraji, M. Emanuel, X. Hong, M. Sherback, V. Agrawal, C. Chipman, and T. Razazan, “20-mW Widely Tunable Laser Module Using DFB Array and MEMS Selection,” *IEEE Photonics Technology Letters*, 14 (10), 1457-1459 (2002).
6. C.-P. Chang, “MEMS for Telecommunications: Devices and Reliability,” *IEEE Custom Integrated Circuits Conference*, 199-206 (2003).
7. P. De Dobbelaere, K. Falta, L. Fan, S. Gloeckner, and S. Patra, “Digital MEMS for Optical Switching,” *IEEE Communications Magazine*, 88-95 (2002).
8. C.J. Wilson and P.A. Beck, “Fracture Testing of Bulk Silicon Micro-cantilever Beams Subjected to a Side Load,” *Journal of Microelectromechanical Systems*, 5 (3), 142-150 (1996).
9. K. Minoshima, S. Inoue, T. Terada, and K. Komai, “Influence of Specimen Size and Sub-Micron Notch on the Fracture Behavior of Single Crystal Silicon Microelements and Nanoscopic AFM Damage Evaluation,” *Materials Research Society Symposium Proceedings*, 546, 15-20 (1999).
10. K.-S. Chen, A. Ayon, and S.M. Spearing, “Controlling and Testing the Fracture Strength of Silicon on the Mesoscale,” *Journal of the American Ceramic Society*, 83 (6), 1476-84 (2000).
11. P. Chen and M.H. Liepold, “Fracture Toughness of Silicon,” *American Ceramic Society Bulletin*, 59, 469-72 (1980).
12. O.N. Pierron and C.L. Muhlstein, “The Critical Role of Environment in Fatigue Damage Accumulation in Deep-Reactive Ion-Etched Single-Crystal Silicon Structural Films,” *Journal of Microelectromechanical Systems*, 15 (1), 111-119 (2006).
13. W.W. Van Arsdell and S.B. Brown, “Subcritical Crack Growth in Silicon MEMS,” *Journal of Microelectromechanical Systems*, 8 (3), 319-327 (1999).
14. V.T. Srikar and S.D. Senturia, “The Reliability of MEMS in Shock Environments,” *Journal of Microelectromechanical Systems*, 11 (3), 206-214 (2002).
15. D.M. Tanner, J.M. Walraven, K.S. Helgesen, L.W. Irwin, F. Brown, N.F. Smith, and N. Masters, “MEMS Reliability in Shock Environments,” *38th Annual International Reliability Physics Symposium*, San Jose, CA, 129-138 (2000).
16. D.M. Tanner, J.M. Walraven, K.S. Helgesen, L.W. Irwin, D.L. Gregory, J.R. Stake, and N.F. Smith, “MEMS Reliability in a Vibration Environment,” *38th Annual International Reliability Physics Symposium*, San Jose, CA, 139-145 (2000).